Neuronal Activity Enhances mRNA Localization to Myelin Sheaths During Development

Katie M. Yergert, Jacob H. Hines[1] and Bruce Appel[2*]

Department of Pediatrics, University of Colorado Anschutz Medical Campus, Aurora, Colorado, 80045, USA

[1]current address: Department of Biology, Winona State University, Winona, Minnesota, 55987, USA

[2]Lead Contact

*Correspondence: bruce.appel@ucdenver.edu, @AppelbhBruce

SUMMARY

Myelin, a specialized membrane produced by oligodendrocytes, insulates and supports axons. Oligodendrocytes extend numerous cellular processes to wrap multiple axons, and myelin sheaths differ in length and thickness. Notably, neuronal activity can modify sheath characteristics. How myelin formation is controlled at sites distant from oligodendrocyte cell bodies is not well known. Using zebrafish, we tested the possibility that 3' untranslated regions (UTRs) influence localization of myelin mRNAs, thereby enabling localized gene expression. By visualizing mRNA in living animals, we found that some candidate 3' UTRs were enriched in myelin sheaths and localized near growth zones of nascent myelin membrane. Injecting zebrafish larvae with tetrodotoxin to block action potentials reduced the amounts of mRNAs localized to myelin in a 3' UTR-dependent manner. Our data indicate that 3' UTRs contain information for neuronal activity-regulated localization of mRNAs to myelin, suggesting that changes in sheath characteristics result from mRNA regulation within nascent sheaths.

Keywords: myelin, oligodendrocyte, mRNA, zebrafish

INTRODUCTION

In the central nervous system of vertebrate animals, axon conduction velocities and axon health are enhanced by myelin membrane. Myelin is produced by oligodendrocytes, glial cells that extend numerous processes to wrap multiple axons simultaneously. Myelin membrane sheaths vary in length and thickness, even when formed by the same oligodendrocyte (Murtie, Macklin and Corfas, 2007; Almeida *et al.*, 2011; Chong *et al.*, 2012), suggesting that molecular mechanisms at the axon-glia interface locally control myelin growth. Notably, neuronal activity is one signal that modulates the length and thickness of some myelin sheaths (Gibson *et al.*, 2014; Hines *et al.*, 2015; Mensch *et al.*, 2015; Etxeberria *et al.*, 2016; Koudelka *et al.*, 2016; Mitew *et al.*, 2018). What are the molecular mechanisms underlying local control of myelin sheath growth in response to neuronal activity?

Transport of mRNA and local translation are broadly utilized mechanisms for controlling subcellular functions. In neurons, many mRNAs occupy axons (Taylor *et al.*, 2009; Minis *et al.*, 2014; Briese *et al.*, 2016; Hafner *et al.*, 2019), dendrites (Cajigas *et al.*, 2012) and growth cones (Zivraj *et al.*, 2010) and are locally translated to control axon growth and synapse formation (Kang and Schuman, 1996; Huber, Kayser and Bear, 2000; Zhang and Poo, 2002; Leung *et al.*, 2006). Frequently, mRNA localization in neurons is determined by 3' UTRs (Taliaferro *et al.*, 2016). RNA sequencing recently revealed that myelin purified from mouse brain has hundreds of transcripts (Thakurela, Garding, Ramona B. Jung, *et al.*, 2016). Many of these mRNAs encode proteins that function in cellular differentiation, translation regulation and cell-cell signaling, which might be important for sheath formation and myelination. Here we describe experiments to test the hypothesis that neuronal activity promotes myelin sheath localization of mRNAs via their 3' UTRs.

RESULTS

mbpa mRNA accumulates at distinct sites within nascent myelin sheaths

Myelin sheaths have transcripts encoding Myelin Basic Protein (MBP) (Kristensson *et al.*, 1986; Trapp *et al.*, 1987; Ainger *et al.*, 1993) but we lack information about the distribution of *MBP* mRNA within sheaths in vivo. We therefore began by using techniques to visualize and quantify the subcellular distribution of mRNA encoded by *mbpa*, a zebrafish ortholog of human and rodent *MBP*. First, we performed single molecule fluorescent in situ RNA hybridization (smFISH) (Femino *et al.*, 1998; Raj *et al.*, 2008) to detect *mbpa* transcripts during early stages of larval development. To mark oligodendrocytes and myelinating sheaths we used *Tg(mbpa:EGFP-CAAX)* larvae, which express a membrane-tethered EGFP under control of *mbpa* regulatory DNA. In the zebrafish hindbrain at 4 days post-fertilization (dpf), a time of active axon ensheathment and myelination (Czopka, Ffrench-Constant and Lyons, 2013), *mbpa* mRNA occupied cell bodies and myelin sheaths (Figure 1A).

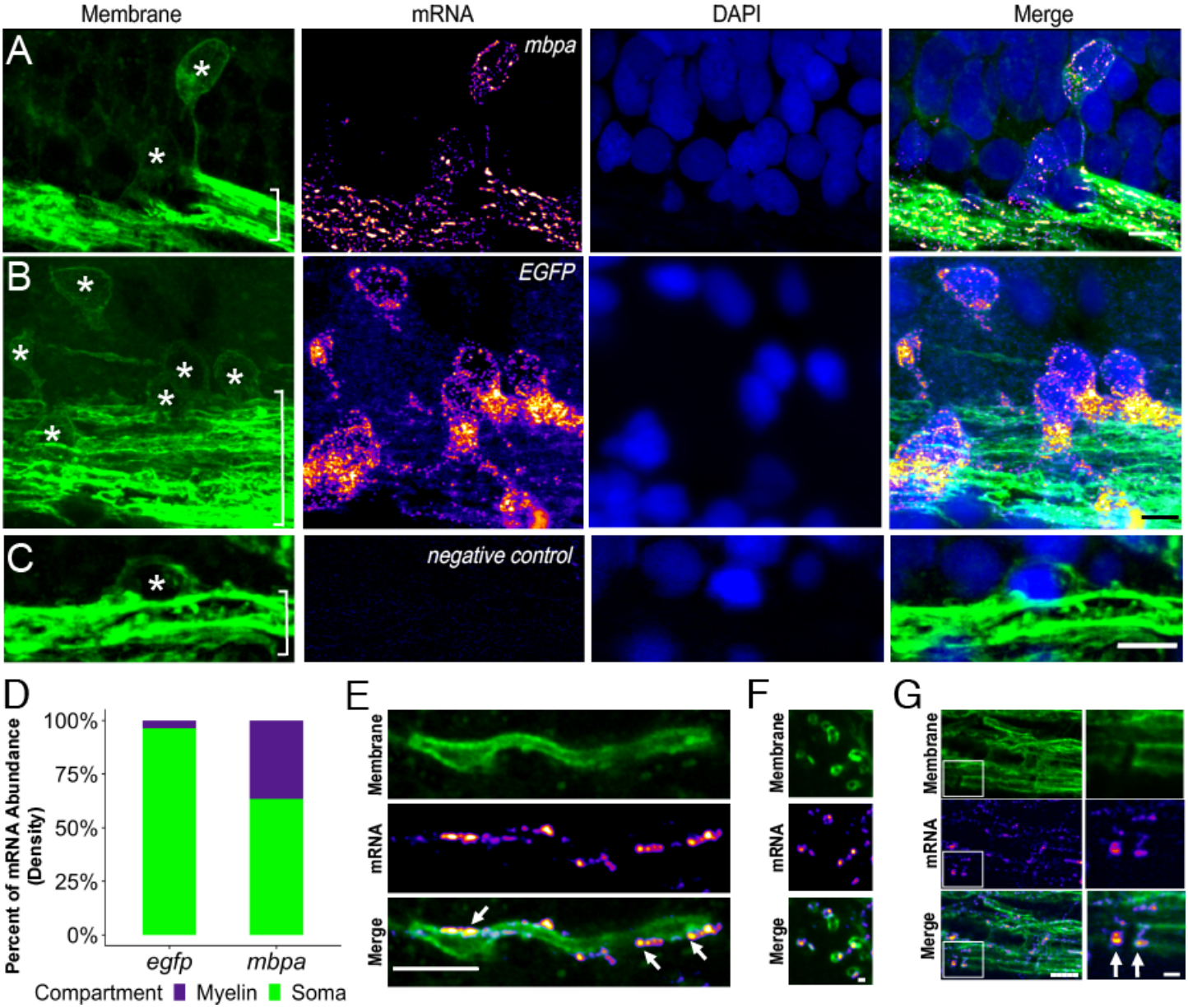

Figure 1. *mbpa* mRNA accumulates at distinct sites within nascent myelin sheaths

(A-C) Representative images of smFISH experiments using 4 dpf transgenic larva expressing EGFP-CAAX to mark oligodendrocytes. Images show sagittal sections of the hindbrain. DAPI labeling reveals nuclei. Sections were treated with smFISH probes designed to detect *mbpa* (A) or *EGFP-CAAX* (B) mRNA. As a negative control, no probe was applied (C). Asterisks mark cell bodies. Brackets mark myelin tracts. (D) Proportion of *EGFP* or *mbpa* mRNA abundance in cell bodies compared to myelin tracts. A minimum (n) for each group was 3 larvae, 11 cell bodies and 21 myelin regions. (E) Images of a single optical section of a myelin sheath in a 3 dpf larva. *mbpa*$^{+}$ transcripts line the myelin sheath. Arrows highlight clusters of *mbpa* mRNA^{+} puncta. (F) Images of a single optical section in transverse plane of myelin sheaths in a 5 dpf larva. (G) Images of a single optical section of myelin tracts in the hindbrain of a 5 dpf larva. Boxed area magnified to highlight sheath termini (arrows). Scale bars, (A-C, E, G), 5 μm; (F, boxed enlargements), 1 μm.

We evaluated *mbpa* mRNA enrichment in myelin by comparing it to *EGFP-CAAX* mRNA expression encoded by the transgene. The 3' end of the *EGFP-CAAX* mRNA consists of a 192 nt polyadenylation signal isolated from simian virus 40, which promotes 3' end formation of exogenous transcripts and does not contain any known localization elements (Fitzgerald and Shenk, 1980; Buj *et al.*, 2013). Similar to *mbpa* mRNA, we detected *EGFP-CAAX* mRNA in cell bodies and myelin sheaths (Figure 1B). Samples processed without probe produced no hybridization signal (Figure 1C). In contrast to *mbpa* mRNA, *EGFP-CAAX* mRNA was concentrated in cell bodies. Measuring mRNA abundance, by calculating the average density of mRNA transcripts, in cell bodies compared to similar volumes of myelin revealed that 37% of *mbpa* mRNA occupied myelin sheaths but only 4% of the *EGFP-CAAX* transcripts were localized to the myelin (Figure 1D). These data indicate that *mbpa* mRNA is selectively enriched in myelin sheaths.

We further examined the distribution of single mRNAs within myelin sheaths. Both longitudinal (Figure 1E) and transverse (Figure 1F) views revealed that *mbpa* transcripts did not uniformly fill myelin sheaths but, instead, were evident as discrete puncta. Multiple puncta frequently appeared to be clustered in larger granules, both along sheaths (Figure 1E) and at sheath termini (Figure 1G). Potentially, these granules represent ribonucleoprotein complexes that regulate mRNA localization, stability and translation.

The *mbpa* 3' UTR localizes mRNA to myelin membrane growth zones

The *mbpa* 3' UTR localizes mRNA to oligodendrocyte processes (Torvund-Jensen *et al.*, 2018). To investigate 3' UTR-dependent mRNA localization in oligodendrocytes of living animals, we adapted the MS2 system (Bertrand *et al.*, 1998; Fusco *et al.*, 2003; Campbell *et al.*, 2015). This system has two components: a mRNA that has a *24xMBS* RNA sequence that forms stem-loop structures and a reporter consisting of the MS2 coat protein fused to EGFP and a nuclear localization signal (NLS-MCP-EGFP), which binds the *24xMBS* stem-loops. We created plasmids that express NLS-MCP-EGFP under control of *sox10* regulatory DNA and a mRNA with sequence encoding mScarlet-CAAX reporter protein, the *24xMBS* and *mbpa* 3' UTR sequences and a *sv40* polyadenylation signal under control of *mbpa* regulatory DNA. When expressed in the same oligodendrocyte, the NLS-MCP-EGFP reporter moves from the nucleus to reveal cytoplasmic localization of the mRNA (Figure 2A). As controls we created plasmids lacking the *24xMBS* or the *mbpa* 3' UTR sequence.

By injecting plasmids at the one cell stage we created mosaic larvae that expressed mRNAs in subsets of oligodendrocytes, permitting visualization of single cells. In the absence of *24xMBS* sequence, NLS-MCP-EGFP was evident in oligodendrocyte nuclei but not in myelin sheaths, which were revealed by mScarlet-CAAX, at 3 and 5 dpf (Figure 2B,C). By contrast, NLS-MCP-EGFP was

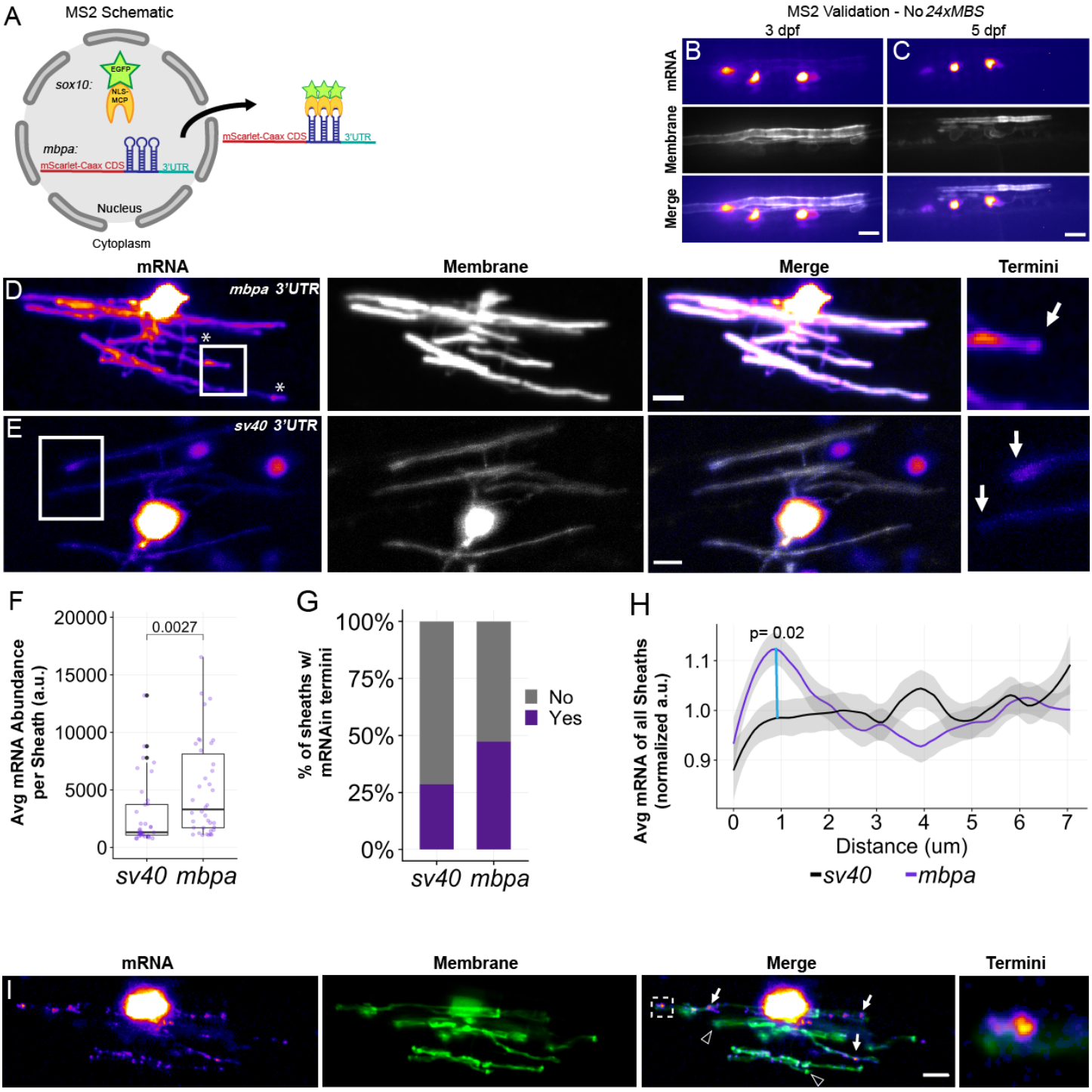

Figure 2. The *mbpa* 3' UTR localizes mRNA to myelin membrane growth zones

(A) Schematic representation of the MS2 system for visualizing mRNA localization in oligodendrocytes. *sox10* drives expression of nuclear-localized NLS-MCP-EGFP (orange crescent and green star). *mbpa* drives expression of mRNA encoding mScarlet-CAAX fluorescent protein with a repetitive sequence that creates 24 stemloops. When co-expressed, the mRNA-protein complex is exported from the nucleus and localized via the 3' UTR. (B-C) Representative images of two myelinating oligodendrocytes expressing mRNA lacking the *24xMBS*. NLS-MCP-EGFP remains in the nucleus at 3 dpf (B) and 5 dpf (C). (D-E) Representative images of localization directed by the *mbpa* (D) or control *sv40* 3' UTR (E). Asterisks mark sheaths with mRNA enriched at

termini. Boxed areas are enlarged to highlight sheath termini (arrows). (F) Average mRNA abundance, measured by EGFP fluorescence intensity, per myelin sheath using the MS2 system. *sv40*: n= 5 larvae, 35 sheaths. *mbpa*: n= 6 larvae, 38 sheaths. (G) Proportion of sheaths with mRNA enriched at the ends of myelin sheaths in 4 dpf larvae. Proportion measured as (sheaths with enrichment / number of sheaths) = 10/35 *sv40,* 18/38 *mbpa*. (H) Average fluorescence intensity across a 7 μm distance from myelin sheath termini at 4 dpf. Each line scan was normalized to the average fluorescent intensity per sheath. All normalized values were then averaged. *sv40* 3' UTR n= 5 larvae, 35 sheaths. *mbpa* 3' UTR n= 6 larvae, 38 sheaths). (I) Representative images showing colocalization of mRNA containing *mbpa* 3' UTR and F-actin in a myelinating oligodendrocyte. Boxes are magnified to highlight sheath termini. Statistical significance evaluated using Wilcoxon test. Scale bars, 5 μm.

localized to the myelin sheaths of oligodendrocytes expressing mRNA containing both the *24xMBS* sequence and *mbpa* 3' UTR sequence (Figure 2D). In comparison to the mScarlet-CAAX membrane reporter, the NLS-MCP-EGFP signal often appeared punctate, particularly at sheath termini, similar to the punctate distribution of *mbpa* transcripts detected by smFISH. NLS-MCP-EGFP signal also was evident in myelin sheaths of oligodendrocytes expressing *24xMBS* mRNA lacking *mbpa* 3' UTR sequence but did not appear as discrete puncta (Figure 2E). Although mRNAs with and without *mbpa* 3' UTR sequence were localized to myelin sheaths, there appeared to be more NLS-MCP-EGFP signal in myelin sheaths expressing mRNA containing *mbpa* 3' UTR sequence than in sheaths expressing mRNA without it. Consistent with the visual comparison, the average fluorescent intensity of sheaths having *mbpa* 3' UTR sequence was approximately two-fold greater than sheaths without the *mbpa* 3' UTR (Figure 2F). Thus, the *mbpa* 3' UTR enhances mRNA concentration within myelin sheaths, consistent with observations that the 3' UTR mediates active mRNA transport (Ainger *et al.*, 1997).

Our smFISH data revealed that *mbpa* mRNA might be concentrated at sheath termini (Figure 1G). Using the dual membrane and mRNA reporters of the MS2 system we determined that about half the sheaths had end-localized *mbpa* 3' UTR-containing mRNA whereas fewer than a third of sheaths had end-localized mRNA in the absence of the *mbpa* 3' UTR (Figure 2G). Plotting the fluorescence intensity values over a distance of 7 μm from sheath ends revealed a strong peak of fluorescence within 1 μm of the ends of sheaths having the *mbpa* 3' UTR construct but not those expressing the control mRNA (Figure 2H). Thus, two independent methods of *mbpa* transcript visualization, smFISH and MS2, reveal mRNA concentrated near the ends of myelin sheaths during the period of sheath growth.

Sheaths with the *mbpa* 3' UTR construct also had a second peak of fluorescence intensity about 6 μm from sheath termini. The peak-to-peak periodicity in fluorescence intensity is similar to stepwise differences in intensity of a membrane-bound fluorescent reporter during developmental myelination, which represents stepwise differences in the number of myelin wraps (Snaidero *et al.*, 2014). Therefore, one possible interpretation of our data is that *mbpa* mRNA is preferentially localized near the leading

edge, or growth zone, of myelin membrane as it wraps around and extends along axons. To confirm this interpretation, we created plasmids to mark *mbpa* 3' UTR-containing mRNA with NLS-MCP-tagRFP and co-expressed them in oligodendrocytes with Lifeact-mNeonGreen, which reveals filamentous actin (F-actin). During developmental myelination, F-actin marks the growth zone or leading edge of nascent myelin membrane (Snaidero *et al.*, 2014; Nawaz *et al.*, 2015; Zuchero *et al.*, 2015). This revealed that most mRNA puncta were closely associated with F-actin (Figure 2I). Together, these data provide evidence that myelin mRNAs are localized near growth zones during developmental myelination.

Different 3' UTR sequences have distinct effects on mRNA localization

Myelin fractionated from mouse brains contains several hundred mRNAs (Thakurela, Garding, Ramona B. Jung, *et al.*, 2016). Do 3' UTRs mediate localization of these transcripts to myelin? As a first step toward answering this question we selected several candidate mRNAs to test using the MS2 system. Our selection process is outlined in Figure 3A. This led us to ten candidates, of which we were able to clone 3' UTR sequences from six genes: *cadm1b*, *cyfip1*, *dlg1*, *eif4ebp2*, *fmr1* and *lrrtm1* (Figure 3B).

The MS2 assay revealed that mRNAs with all six 3' UTR sequences occupied nascent myelin sheaths (Figure 3C). However, there were noticeable differences in the NLS-MCP-EGFP fluorescence intensities produced by constructs having different 3' UTRs. Quantification revealed that mRNAs with 3' UTRs from *eif4ebp2*, *fmr1* and *lrrtm1* produced significantly greater levels of fluorescence intensities in myelin sheaths than the *sv40* control whereas the remainder, *cyfip1*, *dlg1* and *lrrtm1*, were similar to *sv40* (Figure 3D). These data raise the possibility that only a subset of mRNAs in myelin are enriched by their 3' UTRs.

To determine if these 3' UTRs influence sub-sheath localization, we calculated the proportion of sheaths that were marked at their ends by NLS-MCP-EGFP fluorescence. This revealed that constructs with any of the 3' UTRs were localized to sheath ends more frequently than the control construct containing *sv40* sequence alone, with frequencies ranging from 35%-80% (Figure 3E). Additionally, all produced peaks of fluorescence intensity within 1 μm and 6-7 μm of the ends (Figure 3F), similar to *mbpa*. Although these data reveal no clear correlations between sheath enrichment, terminal localization and fluorescence intensity distributions at sheath ends, they indicate that mRNAs that are not enriched within sheaths nevertheless can be enriched near the leading edge of nascent myelin membrane. This raises the possibility that mRNA localization to myelin sheaths and sub-sheath localization are mechanistically distinct.

A

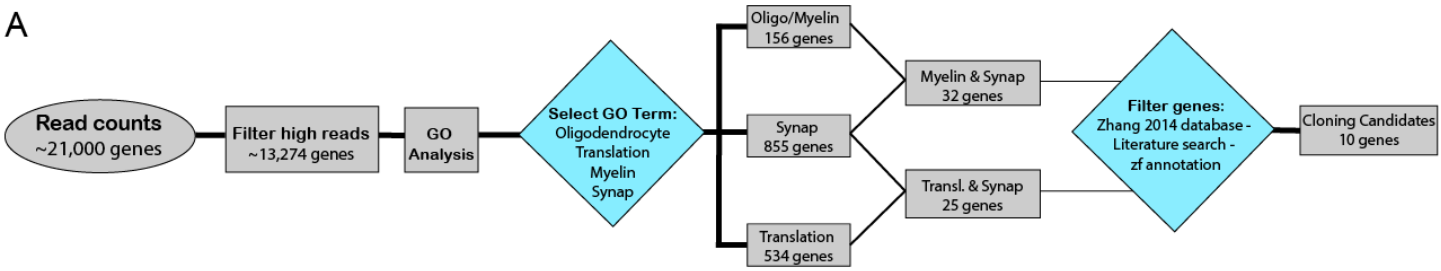

B

Candidate 3'UTRs		
Gene name	Length (nt)	% of 3' UTR
cadm1b	1220	100%
cyfip1	858	88.1%
dlg1	1522	97.2%
eif4ebp2	2282	98.5%
fmr1	2486	99.4%
lrrtm1	368	93.6%

C

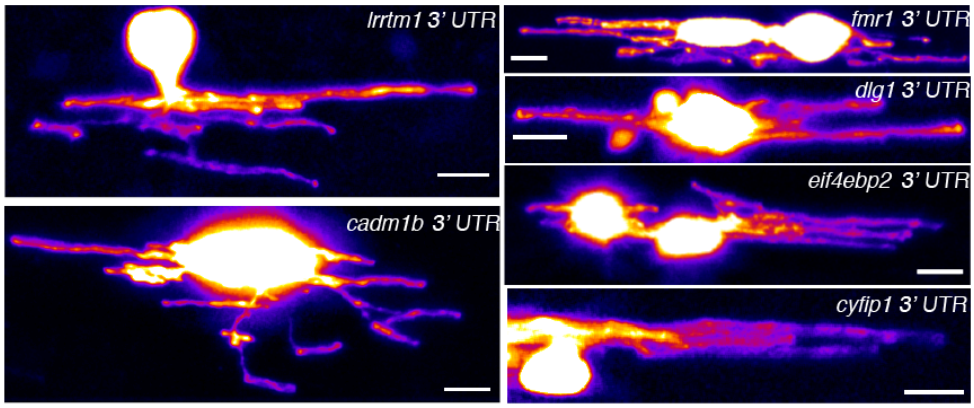

D

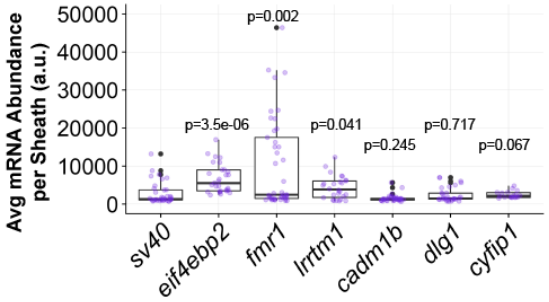

E

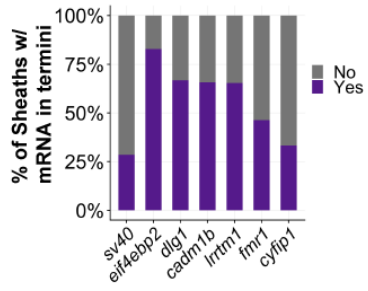

F

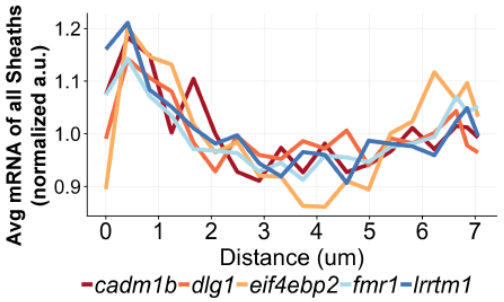

Figure 3. Different 3' UTR sequences have distinct effects on mRNA localization

(A) Work flow to identify target genes from Thakurela et al. 2016. (B) Table listing candidate 3' UTRs incorporated into the MS2 system, 3' UTR length and the percentage of sequence that was cloned based on the annotated genome. (C) Representative images showing localization of mRNAs containing different 3' UTR sequences in oligodendrocytes. Scale bars, 10 μm. (D) Average mRNA abundance, measured by average EGFP fluorescent intensity, per myelin sheath for each 3' UTR. Wilcoxon-rank sum was used to compare groups to control. (E) Proportion of sheaths with mRNA enriched at the sheath ends for each 3' UTR. Proportion measured as (sheaths with enrichment / number of sheaths) = 10/35 *sv40,* 24/29 *eif4ebp2,* 19/41 *fmr1,* 23/35 *cadm1b*, 20/30 *dlg1,* 6/18 *cyfip1*, 17/26 *lrrtm*1. (F) Line scans of the average mRNA abundance (EGFP fluorescent intensity) across a 7 μm distance from sheath termini for each 3'UTR. Each line scan was normalized to the average fluorescent intensity per sheath. All normalized values were then averaged to create the plot. A minimum (n) of 5 larvae and 18 sheaths was used in each condition at 4 dpf (D-F).

Neuronal activity regulates myelin sheath mRNA abundance and localization

Neuronal activity can modulate synaptic mRNA localization (Tongiorgi, Righi and Cattaneo, 1997; Steward and Worley, 2001; Tiruchinapalli *et al.*, 2003; Farris *et al.*, 2014; Yoon *et al.*, 2016). Does

neuronal activity similarly regulate mRNA localization in nascent myelin sheaths? To begin testing this possibility we inhibited neuronal activity by injecting 2 dpf larvae with tetrodotoxin (TTX), which blocks voltage-gated sodium channels and thereby eliminates action potentials (Buss, Bourque and Drapeau, 2003). Whole-mount in situ RNA hybridization revealed that TTX-injected larvae expressed substantially lower levels of *mbpa* mRNA than control larvae (Figure 4A). We confirmed this observation

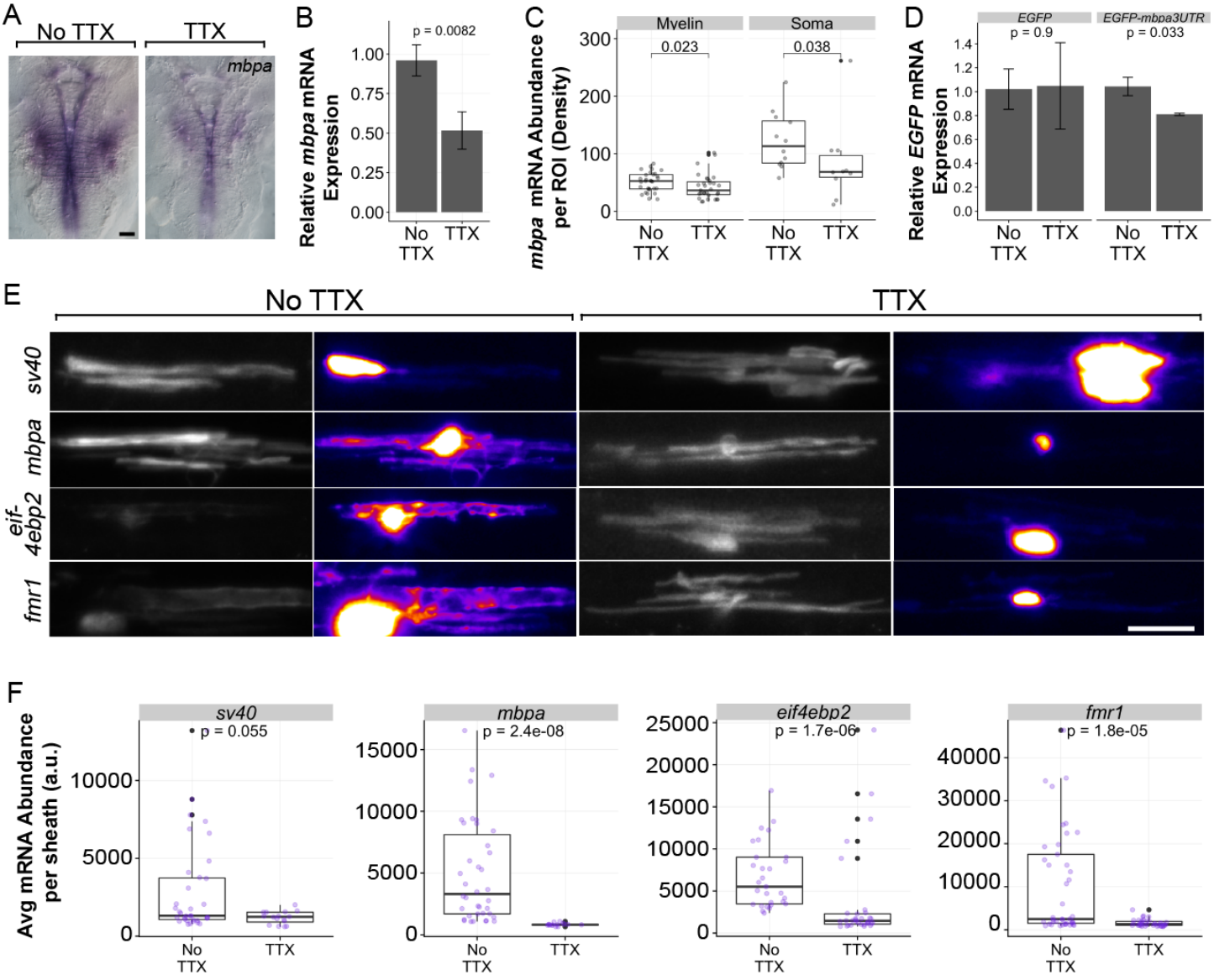

Figure 4. Neuronal activity regulates myelin sheath mRNA abundance and localization

(A) Representative images showing *mbpa* mRNA expression in the hindbrain of control or TTX-injected larvae. (B) Semi-quantitative RT-PCR measurements of *mbpa* transcript levels from whole control or TTX-injected larvae. n= 3 biological replicates. (C) smFISH quantification of *mbpa* transcript levels in subcellular compartments in control or TTX-injected larvae. A minimum (n) for each group was 4 larvae, 5 cells and 15 myelin regions. (D) Semi-quantitative RT-PCR measurements of *EGFP* mRNA levels expressed by *Tg(mbpa:EGFP)* or *Tg(mbpa:EGFP-mbpa 3' UTR)* transgenes in control or TTX-injected larvae. (E) Representative images of myelinating oligodendrocytes expressing MS2 constructs containing *mbpa*, *eif4ebp2*,

fmr1 or *sv40* 3' UTRs in control or TTX-injected larvae. (F) Raw fluorescence intensities for MS2 mRNA reporters in myelin sheaths of control or TTX-injected larvae. Minimum (n) for each group was 2 larvae and 15 sheaths. Statistical analysis performed using Wilcoxon t-test for all comparisons in (C) and (F); Student's t-test in (B) and (D). All experiments performed at 4 dpf.

using semi-quantitative RT-PCR, which showed that the total amount of *mbpa* mRNA was reduced about 50% by TTX injection (Figure 4B). smFISH revealed that TTX reduced transcript density in both soma and myelin compartments (Figure 4C). Thus, normal neuronal activity enhances *mbpa* mRNA abundance within nascent myelin sheaths, consistent with observations that activity promotes myelin membrane growth (Hines *et al.*, 2015; Mensch *et al.*, 2015).

Is the effect of blocking neuronal activity on *mbpa* transcript levels mediated by the 3' UTR? To address this we performed semi-quantitative RT-PCR to measure *EGFP* transcripts in transgenic *Tg(mbpa:EGFP)* and *Tg(mbpa:EGFP-mbpa3'UTR)* larvae. Whereas control and TTX-injected *Tg(mbpa:EGFP)* larvae expressed *EGFP* mRNA equally, TTX reduced the amount of *EGFP* mRNA expressed by *Tg(mbpa:EGFP-mbpa 3' UTR)* larvae relative to the control (Figure 4D). This result shows that TTX-sensitive neuronal activity does not influence the transcriptional activity of the 2.6 kb of *mbpa* genomic regulatory DNA used in our experiments but that, instead, neuronal activity must influence *mbpa* transcript abundance via the 3' UTR.

We used the MS2 system to further investigate the role of 3' UTRs in mediating the effects of neuronal activity on transcript localization. To establish a baseline, we first measured fluorescence intensity from myelin sheaths expressing the *sv40* control construct. TTX treatment slightly reduced the abundance of the control mRNA (Figure 4E,F) in myelin sheaths, although a statistical assessment comparing expression to untreated larvae indicated that the difference was modest. By contrast, TTX-injection significantly reduced the myelin sheath abundance of mRNA containing the *mbpa* 3' UTR (Figure 4E,F). Similarly, TTX significantly reduced the myelin sheath abundance of mRNAs containing *fmr1* and *eif4ebp2* 3' UTRs (Figure 4E,F). Thus, for select transcripts, 3' UTR sequences enhance myelin sheath abundance in response to neuronal activity.

DISCUSSION

Although myelin membrane localization of *MBP* transcripts is well-documented (Kristensson *et al.*, 1986; Trapp *et al.*, 1987; Ainger *et al.*, 1993), we found new features of localization within sheaths. Specifically, *mbpa* transcripts often were concentrated near the growth zones of nascent myelin membrane. What accounts for enrichment near growth zones? Whereas *MBP* mRNA is transported on microtubules through the major oligodendrocyte processes (Carson *et al.*, 1997; Lyons *et al.*, 2009; Herbert *et al.*, 2017), myelin sheaths lack microtubules and therefore microtubule-based transport likely

is not the primary mode of mRNA localization within myelin. Myelin sheath growth zones are marked by F-actin (Nawaz *et al.*, 2015; Zuchero *et al.*, 2015), which also can facilitate mRNA transport, mediated by myosin motor proteins (Bertrand *et al.*, 1998; Yoshimura *et al.*, 2006; Krauss *et al.*, 2009). Growth zone localization might also indicate sites of local protein translation. In support of this possibility, purified myelin contains a free ribosome fraction (Colman, 1982), electron micrographs revealed ribosomes in the distal ends of oligodendrocyte processes (Lunn, Baas and Duncan, 1997) and a MBP reporter protein was translated in processes of cultured oligodendrocyte precursor cells (Wake, Lee and Fields, 2011). Our own work indicates that proteins characteristic of post-synaptic complexes, such as PSD95, are concentrated near myelin sheath growth zones (Hughes & Appel, submitted), raising the possibility that growth zones are sites of axon-oligodendrocyte signal transduction that regulate local protein synthesis. Testing this model directly will require methods for visualization of protein synthesis in vivo (Halstead *et al.*, 2015; Morisaki *et al.*, 2016; Pichon *et al.*, 2016; Wang *et al.*, 2016; Yan *et al.*, 2016).

Although all six new mRNAs that we tested were discovered in myelin by RNA sequencing (Thakurela, Garding, Ramona B. Jung, *et al.*, 2016), the 3' UTRs of only three were enriched in sheaths relative to a control mRNA. Thus, for some mRNAs, cis-regulatory elements important for mRNA localization might be embedded in 5' UTRs or coding regions of the transcripts or, alternatively, many transcripts might occupy myelin by diffusion. Notably, whereas the myelin sheath abundance of mRNAs that were not enriched were uniformly similar to the *sv40* control, the level of mRNA enriched in individual sheaths varied widely (Figure 3D). For example, the sheath abundance of *fmr1* appeared to be bimodal, with some sheaths equivalent to the control but others having considerably greater amounts. This raises the possibility that there is heterogeneity in axonal control of myelin sheath mRNA localization, whereby only specific axonal subtypes provide mRNA-regulatory signals to proximate myelin sheaths. Potentially, these axonal subtypes correspond to axons myelinated by vesicle secretion-dependent or -independent mechanisms (Koudelka *et al.*, 2016).

Following evidence that neuronal activity can modulate mRNA levels near synapses (Yoon *et al.*, 2016), we investigated the possibility that neuronal activity also affects mRNA levels in nascent myelin sheaths. Blocking action potentials caused significant reductions in the amounts of mRNA localized to sheaths containing 3' UTRs from *mbpa, fmr1* and *eif4ebp2*, and our data indicated that these effects were independent of changes in transcription. For each mRNA, TTX treatment reduced sheath amounts to the level of the control, in contrast to the wide distribution of individual sheath mRNA amounts evident in untreated larvae (Figure 4F), again consistent with the possibility that interaction with different axons can differently regulate localization of transcripts to individual myelin sheaths.

Notably, two transcripts that were enriched in myelin sheaths by 3' UTRs and neuronal activity, *eif4ebp2* and *fmr1,* encode proteins that regulate translation. Upon phosphorylation, EIF4EBP2 dissociates from EIF4E, thereby enhancing translation (Pause *et al.*, 1994; Banko *et al.*, 2005; Gkogkas *et al.*, 2012). Thus, sheath-localized EIF4EBP2 might regulate myelin mRNA translation during development. FMRP, an RNA binding protein encoded by *fmr1* and inactivated in Fragile X Syndrome, regulates mRNA stability and translation (Li *et al.*, 2001; Zalfa *et al.*, 2003, 2007). FMRP binds *MBP* mRNA (Wang *et al.*, 2003) and myelination is delayed in a mouse model of Fragile X (Pacey *et al.*, 2013). Our data therefore raise the possibility that activity-regulated localization of *eif4ebp2* and *fmr1* transcripts to myelin sheaths contributes to modulation of sheath characteristics.

ACKNOWLEDGMENTS

We are grateful to Florence Marlow for her generous gift of the MS2 plasmids. We thank Karlie Fedder and Douglas Shepherd for their guidance during smFISH quantification. We thank Matthew Taliaferro, Caleb Doll, Stephanie Moon and RNA Bioscience Initiative fellows Austin Gillen and Kent Riemondy for their comments. This work was supported by US National Institutes of Health (NIH) grant R01 NS046668 and a gift from the Gates Frontiers Fund to B.A., a National Multiple Sclerosis Postdoctoral Fellowship (FG 2024-A-1) and NIH (NIMH) fellowship T32 MN015442 to J.H.H. K.M.Y was supported by NIH (NIGMS) T32 fellowship GM008730 and as a RNA Scholar of the RNA Bioscience Initiative, University of Colorado School of Medicine. The University of Colorado Anschutz Medical Campus Zebrafish Core Facility was supported by NIH grant P30 NS048154. All DNA plasmids and transgenic zebrafish used in this study are available by request.

AUTHOR CONTRIBUTIONS

K.M.Y. and B.A. conceived the project. K.M.Y. performed all the experiments and collected and analyzed all the data with the exceptions of the whole mount *mbpa* in situ RNA hybridization and the *EGFP* semi-quantitative RT-PCR experiments, which were performed by J.H.H. J.H.H. cloned the *mbpa* 3' UTR sequence and created *Tg(mbpa:EGFP-CAAX-polyA-CG2)*^{co53} and *Tg(mbpa:EGFP-mbpa 3' UTR-tol2)*$^{co54.}$ K.M.Y. and B.A. wrote the manuscript.

DECLARATION OF INTERESTS

The authors declare no competing financial interests.

STAR METHODS

CONTACT FOR REAGENT AND RESOURCE SHARING

Further information and requests for resources and reagents should be directed to and will be fulfilled by the Lead Contact, Bruce Appel (bruce.appel@ucdenver.edu).

EXPERIMENTAL MODEL AND SUBJECT DETAILS

Zebrafish lines and husbandry

All procedures were approved by the University of Colorado Anschutz Medical Campus Institutional Animal Care and Use Committee (IACUC) and performed to their standards. All non-transgenic embryos were obtained from pairwise crosses of male and females from the AB strain. Embryos were raised at 28.5°C in E3 media (5 mM NaCl, 0.17 mM KCl, 0.33 mM CaCl, 0.33 mM $MgSO_4$ at pH 7.4, with sodium bicarbonate) and sorted for good health and normal developmental patterns. Developmental stages are described in the results section for individual experiments.

The transgenic line *Tg(mbpa:EGFP-CAAX-polyA-CG2)*^{co53} *and Tg(mbpa:EGFP-mbpa3' UTR-polyA-tol2)*^{co54} were created using Gateway tol2 kit (Kwan *et al.*, 2007). Specifically, p5E-*mbpa* contains 2.6-kb genomic fragment of zebrafish *mbpa* (Hines *et al.*, 2015). *pME-EGFP-CAAX*, *p3E-polyA or p3E-mbpa 3' UTR* and *pDEST-tol2-CG2* were obtained from the Gateway tol2 kit (Kwan *et al.*, 2007). All entry vectors and destination were combined using LR clonase and transformed into DH5α cells. Colonies were screened by enzymatic digestion using BamHI, KpnI, and XhoI. Plasmid DNA was injected into AB embryos which were screened for transgenesis and outcrossed to create transgenic lines. All *Tg(mbpa:EGFP-CAAX-polyA-CG2)*^{co53} and *Tg(mbpa:EGFP-mbpa3' UTR-polyA-tol2)*^{co54} used in these experiments were from F3 or later generations.

METHOD DETAILS

Candidate 3' UTR selection

To select 3' UTR targets for cloning into the MS2 system we utilized published transcriptomics data (Thakurela, Garding, Ramona B Jung, *et al.*, 2016). We downloaded Supplementary Table 1 containing transcript abundance in four stages of myelin development identified by RNA-sequencing. We selected the three biological replicates from P18 for analysis because this developmental timepoint was the most similar to our model. We filtered these data for transcripts with normalized read counts greater than 20 for all 3 biological replicates (representing 21,937 genes). We put all gene names into a gene ontology analysis (geneontology.org) and analyzed the genes for biological processes in Mus musculus. From these biological processes, we copied all genes into an Excel document that fit the term "synap",

"translation", "myelin" and "oligodend". Biological terms identified in gene ontology analysis are listed in Table 1.

Table 1: List of Biological Process for GO Terms

"Synap"	"Translation"	"Myelin"	"Oligodend"
Regulation of Synaptic vesicle cycle	Translation	Regulation of Myelination	Oligodendrocyte Differentiation
Regulation of trans-synaptic signaling	Positive Regulation of Translation	Negative Regulation of Myelination	-
Synaptic Signaling	Regulation of Translation	Ensheathment of Neurons	-
Synaptic Plasticity	Negative Regulation of Translation	Paranode Assembly	-
Synaptic Vesicle Cycle	-	Myelin Assembly	-
Synaptic Vesicle Localization	-	Central Nervous System Myelination	-
Synapse Organization	-	-	-
Positive Regulation of Synaptic Transmission	-	-	-
Regulation of Synapse Structure or Activity	-	-	-

After removing duplicate genes, the "Synap" list contained 855 genes, the "Translation" list contained 534 genes, the "myelin" list contained 128 genes and the "oligodend" list contained 28 genes. To further narrow our search, we cross-referenced these lists with one another to find genes that were common to more than one list, which resulted in 55 genes. To further narrow this list, we cross-referenced these genes with the Brain RNA Seq online database (Zhang *et al.*, 2014) to identify those with evidence of oligodendrocyte lineage cell expression. We next referenced these genes with the zebrafish genome browser (GRCz11) and searched for annotated 3' UTRs for each. Finally, we performed literature searches for published data that were relevant to our model. This resulted in a final list of ten: *dlg1, cyfip1, eif4ebp2, fmr1, cadm1, lrrtm1, eif4g1, eif4a3, mtmr2* and *nfasc*.

3' UTR cloning

To clone the *mbpa 3' UTR*, 5 dpf cDNA from zebrafish larvae was used for PCR amplification using primers to target the flanking regions of the *mbpa* 3' UTR. The PCR fragment was cloned into pJC53.2 using TOPO cloning kit. Colonies were screened by colony PCR. Using Gateway cloning, the *mbpa 3' UTR* was amplified and inserted into pDONR-P2R-P3 using BP clonase. *p3E-mbpa 3' UTR* was confirmed by sequencing.

To clone the additional 3' UTRs, cDNA was created from pooled 6 dpf AB larvae treated with 1 mL of Trizol and snap frozen. All RNA isolation steps were performed on ice and in a 4° centrifuge at 18,078 x g. Larvae were thawed on ice and homogenized with a 23 g needle. 200 µL of chloroform was added and shaken for 15 seconds followed by centrifugation for 10 min. The aqueous layer was transferred to a new tube and an equal volume of 100% cold isopropanol and 2 µL of glycogen blue was added to the sample. The tube was incubated at -20° for 20 min and centrifuged for 10 min. The supernatant was removed and transferred to a new tube and 200 µL of cold 70% ethanol was added to wash the pellet followed by 5 min centrifugation. This step was repeated. After the pellet dried, the RNA was resuspended in 20 µL of molecular grade water. RNA was quantified using a Nanodrop. To synthesize cDNA, we used manufacturer instructions from the iScript™ Reverse Transcription Supermix for RT-qPCR, which uses random hexamer primers to synthesize cDNA.

To amplify the 3' UTRs from cDNA, we designed primers that flanked the annotated 3' UTR as predicted by *Danio rerio* GRCz11 annotated genome. Primers were flanked with attB sequences (Table 2) for cloning into the pDONR-P2R-P3 vector of the Tol2 Gateway kit (Kwan *et al.*, 2007). cDNA was used as a PCR template to amplify the 3' UTRs with primers. Of the ten 3' UTRs we attempted to amplify we were successful with the six listed below. Following amplification, bands were gel extracted using a Qiagen Gel Extraction Kit and cloned into pDONR-P2R-P3 using BP clonase. Clones were verified by sequencing using M13 forward and M13 reverse primers. The p3E-*dlg1* 3' UTR was not fully sequenced due to highly repetitive sequences. We sequenced approximately 51% of the construct from 1-54 and 775-1552 base pairs. We therefore confirmed p3E-*dlg1* 3' UTR identity using restriction mapping.

The *sv40* 3' UTR is a transcription termination and polyadenylation signal sequence isolated from Simian virus 40. We obtained this sequence from the Tol2 Gateway-compatible kit where it is referred to as "pA". This sequence was cloned with Gateway BP clonase into pDONR-P2R-P3. The p3E-sv40 3' UTR was confirmed by sequencing.

Table 2. Primers for UTR amplification and cloning

3' UTR name	Forward Primer (5'->3')	Reverse Primer (5'->3')	3' UTR Length (nt)	Percentage of annotated 3' UTR cloned
lrrtm1-201	GGGGACAGCTTTCTTGTACAAAGTGG TATCCACCCATGTCAGTTTTTACAAAT CAATG	GGGGACAACTTTGTATAATAAA GTTGTTGTTTTCCACTTCAATT GTGTCTGTTCG	368	93.6%
fmr1-201	GGGGACAGCTTTCTTGTACAAAGTGG TACCTTCCCCTCATTCTCCCACT	GGGGACAACTTTGTATAATAAA GTTGTTTGCAGAGGAAGATCAA CCTTTATTTATTGAAA	2486	99.4%

eif4ebp2-201	GGGGACAGCTTTCTTGTACAAAGTGGTAAGAAGAGGAACCTACGTGAACAAC	GGGGACAACTTTGTATAATAAAGTTGTGTCCACTGGCATTGGCA	2282	98.5%
dlg1-201	GGGGACAGCTTTCTTGTACAAAGTGGTAGGGGCCGAAGACAAATAAACCT	GGGGACAACTTTGTATAATAAAGTTGTATGGAATGAATCAAGTTGGCAGATTATGTAC	1522	97.2%
cyfip1-201	GGGGACAGCTTTCTTGTACAAAGTGGTAGCACCAGTTTGAAGTGGAAGAGAT	GGGGACAACTTTGTATAATAAAGTTGTAAAAAGGCACGTTTATGAGGAGTAAGAAC	585	88.1%
cadm1b-201	GGGGACAGCTTTCTTGTACAAAGTGGTACTGGAACTAGACCTGTTAGCTTCC	GGGGACAACTTTGTATAATAAAGTTGTCATTTTAAACTGCTTTTATTCACTGTTATAATT	1220	100%

MS2 plasmid construction

All MS2 constructs were created using Gateway cloning. pME-*HA-NLS-tdMCP-EGFP* and pME-*24xMBS* were generous gifts from Dr. Florence Marlow.

To create pME-*mScarlet-CAAX-24xMBS*, we obtained plasmid pmScarlet_C1 from Addgene. In-Fusion™ cloning was used to assemble mScarlet-CAAX in puc19. Next, we amplified mScarlet-CAAX sequence using primers 5'-GGGGACAAGTTTGTACAAAAAAGCAGGCTTAATGGTGAGCAAGGGCGAG-3' and 5'-GGGGACCACTTTGTACAAGAAAGCTGGGTTTCAGGAGAGCACACACTTGCAG-3' and cloned it in plasmid pDONR-221 using BP clonase to create pME-mScarlet-CAAX. Next, we designed primers flanked with BamHI cut sites (5' -TCCGGATCCATGGTGAGCAAGGGCGAGGCAG-3' and (5'-CGACTCTAGAGGATCGAAAGCTGGGTCGAATTCGCC-3') and PCR amplified the mScarlet-CAAX sequence. We purified the amplified product using QIAquick PCR Purification Kit and digested it with BamHI-HF. pME-*24xMBS* was linearized with BamHI-HF and treated with Antarctic phosphatase to prevent religation. We performed the ligation with 2X Quick Ligase and the ligation reaction was transformed into DH5α competent cells. Clones were screened using restriction mapping, then sequenced for confirmation.

For expression plasmids containing various 3' UTRs, we used Gateway multi-site LR clonase to combine entry vectors with pDEST-tol2. The resulting expression plasmids included: pEXPR-*mbp:mScarlet-Caax-24xMBS-mbpa 3'UTR-tol2*, pEXPR-*mbpa:mScarlet-Caax-24xMBS-lrrtm1 3'UTR-tol2*, pEXPR-*mbpa:mScarlet-Caax-24xMBS-fmr1 3'UTR-tol2*, pEXPR-*mbpa:mScarlet-Caax-24xMBS-eif4ebp2 3'UTR-tol2*, pEXPR-*mbpa:mScarlet-Caax-24xMBS-dlg1 3'UTR-tol2*, pEXPR-*mbpa:mScarlet-Caax-24xMBS-cyfip1 3'UTR-tol2*, pEXPR-*mbpa:mScarlet-Caax-24xMBS-sv40 3'UTR-tol2* and pEXPR-*mbpa:mScarlet-Caax-24xMBS-cadm1b 3'UTR-tol2*. LR clonase reactions were transformed into Stellar Competent Cells (Takara cat # 636763). Clones were screened using restriction mapping.

For control experiments to determine the specificity of mRNA detection by MCP-EGFP, we created an expression plasmid that lacks the 24xMBS stem loops (pEXPR-*mbpa:mScarlet-Caax-mbpa 3'UTR-tol2*).

Lifeact Cloning for F-actin reporter

The filamentous actin reporter was created using Gateway cloning. Alexandria Hughes created pME-lifeact-mNeonGreen by PCR amplification using primers 5'-ggggacaagtttgtacaaaaaagcaggctaccatgggcgtggccgacttga-3' and 5'-ggggaccactttgtacaagaaagctgggttcttgtacagctcgtccatgccca-3' from mNeonGreen-Lifeact-7. We then combined entry vectors and pDEST-tol2 using LR clonase to create pEXPR-*mbpa:lifeact-mNeonGreen-polyA-tol2*.

3' UTR sequences used for MS2 RNA localization experiments

sv40 3' UTR

5'-

gatccagacatgataagatacattgatgagtttggacaaaccacaactagaatgcagtgaaaaaaatgctttatttgtgaaatttgtgatgctatt
gctttatttgtaaccatt
ataagctgcaataaacaagttaacaacaacaattgcattcattttatgtttcaggttcaggggggaggtgtgggaggtttttt -3'

mbpa 3' UTR

5'-

cttctccaagcaggaaaacactgagatggaagagagtgaaatggacggaaagcaaaaacttgagagggaggatgtctgccctacagact
caccagtcgcagcga
gtttaacagactaacattggccatcttcgcttcctagatagagatacaatccaagtatctgttgctacatgcctgcagggttacagaagcacgtgtt
gactgtatgtgtgcaaacttgctgtaataattgtcaatggtcaggtgatgcgatacatcttgtaagtctccctttaaaatttagctgaagtgatcaattt
caatatatacaaagagcaaaaactcatacaaaaggtttgaaacaattagacagagtatttctctttttttaaaatccctgaaccaaccagatgaa
tcatttgatcattctgaattggtcttatatgtgtttcacaaaatggattgcttatatgctctccagcatttgatgtgtggcatttattctatgttatactgcctct
ccatggttttcttgagatccatgttcaacctcatgtgatgtgcatttctgtatgtttgtgttcactgtggtctttgtgttgcattctatattggttatttactttata
ccaggaatttgtatataggaatctttattgagttttaattaatgcaaaaaaaaatatgatgaccagttaactacattaaatttgattcattttgagaaat
gatttagctcttaatcaggaccatgccttaaaatgattaaaaacagactaaaaacacaattttgtggactagggaatagattctaagcatgtatgt
ggcttggattgtatgccctcagatgttgcactgcagtatgtgtgttaaaaccacctgtaaatgttgtctgcgtcattacatgtgcaattttggtgttatttt
agaaaggtctcgtaattaccaggggtaggattaatatttaaataacaaacatgcagaaatctaggacaaagagtcagtgggagcataaagg
aaagggtatgaaaaaaaggaaggaaaacctgaaagtgcaagatggataatgtgggaaatgctaaatgaggacttctgaaagagtaaggt
ggagtttattcagctgatttttttttctttttctgtgttgtatctcatgtgtcttaatatcgttcattgttctgtgtctcatatactctgcc- 3'

eif4ebp2 3' UTR

5'-

aagaagaggaacctacgtgaacaacgattaattacctggtacctgtgtgccagtggcttggcttgtagataccaatgttgtgagccctctccttta
gctctctctagctgctg
ggtgctgtttaatcatggggataaatgactaaagtttgcccagtggtgttgctggagccctgaaagttaacctgtgagccctgttgagctcttctttttt
gttgtttaggtttcagggctgccatcagcagtacttgcttgagtcacagagcaagggaaaaattctctattgcaagtgcccggatatattaccaatt
taccataatagactcataaacggatcagccattagagattcactgctgatagatcaaagtacactgttccagttgatgcccttaatgcagtctattt
cgttcacacataaactgatttgcaggacatgcggttatcattatctccctatattttcgattgtttttccccccagttaattttaaaagggacaacaggatt
atattcatatttttttgattcaaaaagtgaaaaaattccaatcattcctgctcttttatatcatttttttttttcacctcaatacatttttcaggtgttcaaaagaa
tagttttatattgttgtccaaaaatgcataattaaaccattgaccttaatcattcatttgaactgacacatgatttcaatgccaaatgtgcacagaattt
ctcattttatttaggactaccccaaaataagcatttcaggtcatattagtttaatttcccagttttttcactgttaattttaagaaaagaaacacctaatc
acattcgtgaaagaccaaactgttactttagattaaagagaatgtttctgttcagatttattttgctaacagtaaggtttgtttctttgtttgtctttgagag
atgaagcgtcaacatagcctagttaaaagttaataacaccaagtaatgtttgattggataaagggtttaatataccttataagatgttgacaaaga
aagctggtctcaggaagcacttgctttatgcacctaacaattacgcatcttacggctcctgttacgggagaaaaagcacggtgaatatttaacatt
aatatcagctgtgacatctgctgttactttccgaaatactacaatcctcacgaaccttgataatcaaatcaaaggtaggaaagcactgaagtgtt
gttttggtcatcgtaccatcggtctgtctcataagcgcacacaatgtgaacgagttttgtcgcgagcagacattcattttgattcagatcaaacgtct
cgaaaacttgaattgaatctttccaatgctcttctatgcatgttctttcggtctgcttcttaagctttagttcacatgtcagatcattttaacgttgttgttttg
gggggggacgccaaatcgtgtggaagacgagaattattattgtaagagaattaagcaaagagattattcaaacaaagtgacttaaagagga
taagacttattctcatgactttaattgtctttttctgtgctccagtctttgtctgaggcacagaatgatttatttttcctctcacagtgatctcttgtgcttagc
ctccgtatccatgccttactttactaagctgagcagctgtgtcaaatacagtacccttcataccttaaaacgggatcagttcctttctttcgtttctttca
agtggagaacaagatcaagatattgctgttttactagaaaacatttatatttttggagacatgtttgttatcatttactttcttacagaaatgggacgatt
tggaaatgcagaggtgtaatatttgtaatagtaatggattggttaaaagcaaatacagaatttaggtttgactttgaggtcacagttaagtttctattc
aattttgagaacttgtagaatccttggagtatgttttcatgtccggtttgcgcaaaagtcacattcaagttctaatgatttacagtgaagggaaattgg
tgtatactgtccttctgtaatggatatgaatggtcaaattccagcttgtttcaactctaaaattatgaaatgttaaatttttttatttaaaaaaaaataatg
cttactattgctttatgctttccccacgcatcaaactatcagaaatgcatttagttctgtgtgaggggatttaagatggacgtgttttatctaatatggca
aaaaacattggaaactgtattttctttcttctttgaccctgttaattttaatgaaatgccaatgccagtggacac- 3'

lrrtm1 3' UTR

5'-

tccacccatgtcagtttttacaaatcaatgtacgggtggatatggaacatacgttaacttggcacccaattttgctgctctcaaagggagctacagt
tctggagtgtgagtgg
actacaaacatggatttagagctgatttcaacagcctcatggggaaatctgactgtgagacccgtgcacttgatgcaaaagatgtggaatgatt
atgctgaccagtcctggcttctcttgtgaaaagtggatatttgagctttaacgtgtctttctacttcaggatattctaggactctctaaagctaccgagg
acatcaagtacaccatggtaacaaacatacgaacagacacaattgaagtggaaaacaacaa- 3'

fmr1 3' UTR

5'-

ccttcccctcattctcccactcagctccaccaatccagatgcttcttcattagagacacattaggccaaagagaaccaggtcagtagggctgtcg
caagacatgacata
aagcacactttgtaattgttagcggggttaaaagacaaggtctcttggtgtacggtgtgttgaatttggtagtcttcacggattagagagaccggtc
tctaaatctcaactgaagctacaggttttctaattgactttctaaataactacctaaagaagctgtggataaaatgtctctcataaatggaataaaa
acaaaaaaaagagcttttccaagaaattggtttttaaagtttgttttccacaatgtccaaaaaaaagggaaagaaacgcatcggaggatgaac
tcaagctctcgacgcccaagtttatgccacatctcatggcatacattgtttttacacgctttggtgtccatggtttctcgagcccattctgatgtgagat
cttaaccacatcattagcaaaaaaatacaaaaaaaatttaaaaaacgaagagaaaaaataagtaaaaaataaaaaaaatgctcctgtctg
gatctgtgcctttaactagtgtggatagtatcataatttggatgtttaaatcagggaagaaggcgtgaacaacacctgtcacctgagcagagtttg
ttgcaatctcagccgacaactttaaaaacaaacaaaaaaaggtgtttctttttttttctctgtgctgcatgtatttcacaaacattttgtatgtctgaaaa
gcaggattggaaatctattttgccatagctgagttgtgagtagtaaaggtattagcctaactaaactagtcaactgtggaagtcattgattgtaact
aaccacccgagttgaatatcaatgctaattcaacaatgaaagcattaatgaagattaatttgatgtaaagcatatctttgcattttagaacaattgtt
ttttgttttcaatagaggtagcaaagcagtttccttaaacaaaatgtcttttgttttttacttgttttacctccatcatgatataaaggtgaatttgctcaga
tgttttctcacaaacagggtggaaatgctctattttgtttcatttttttttttttgttcatgctggccacagtaaactgccatctttcctgctgtatttttcagcatc
aggtgtgaagcacttatatcagattatatctgtaacattgtctttgtcctaacaatggctcatcatagactgaaaatgttgaactgtgggattgcatac
tgtatattattacatcatccgttaagagattgttgctgttctttttagattgaactttaaatgtgcacttatcatgtttgtgttactctgcaagtactttataatc
tataaacctataataaactagaatgtgataagacttcttcagcaggtgaatcacatgtatgctgtcaacataactaaactgaagtttagatctcttc
gctaattttgagtctactgtacttttgcagcttcgagagggacgagatttgggggaaacacaacgttaactttgatatgaggagaacaaaatgtct
atcttatccgattagtgcttgtgcattaaactttagtttacaattttgagaagacgcaaagctgttctaaacccacgattcttttgaaacctactgtgac
ggtaaacatggtagttttttgactgtacagcaagaaagccagtcagttgtatcctctttgctccttttttcttaacaactctttttcattttatgctcgctagt
caaatatccagctctacctgtaaagcttacaccagtttcaaagtgattttgccttgatcagtgtcctgtgaaaaccaaacggaaggggttacgtttc
acgcgaaatgcaaaaaaaacctgtgactggcagaggatttgcagctctgtgggatgggaatgataaaccactcgaacggggcgtcctggct
gcatccggccccctttaaaatttagcctttatttggaagtaaggtgttaaaatggtttactcccagtatttttaaaaaaacttgcacatctacggtgtg
cagtaaactggcaagatggcagagttcaccagtctgttaaaaaaaaaaaaaaaaaaaaccctttgaagtgttgccaaacagactgttttctagt
tatttatttttttggaatgtatatgaaaaatgacaaattgtaaaaccatctcttgcacacatcgttaggctattgtgatttgaataaagagctgaaaagg
aataaaaacaaacaaaaaacatgaaatactgtagatactgaaccgaggtagactgaccttgtatgttactgcactttgggtgataatttctttgta
cataatagcagaacagactgggttttatgttgacattgtttggttatagtgcaatatattttgtatgcaagcagtttcaataaataaaggttgatcttcct
ctgcaa- 3'

dlg1 3' UTR

Note: dlg1 3' UTR contains highly repetitive sequences that were unable to be fully sequenced. We sequenced approximately 51% of the 3' end. To further confirm our cloning strategy by performing enzymatic restriction digests for the correct size. The sequence below is from the annotated zebrafish genome browser (GRCz11) with our confirmed sequencing from 1-54 and 775-1522 bp.

5’-

ggggccgaagacaaataaaccttacacttcttttaacttttgtatttttttttttaatctttctgtttccttttttttaatattaacatggcctgcagcttgcattgg
ctttccaactcctgagc
ataagaaatgcgttttctttgaatgggtttggggtttttcctctttctctcatgcctctctttgaaactactgtctagaactcgcatcccaatctccgcatgt
ggtcctccactgggaggagacgtgcttgaccagcgacttactggacagattatacggtacagattccttaatgtttaagggaggtgactttctcg
aaggaaaaccaataagttaatgcattatacacattttggtttgttcttcatttttttacccccccagtatatgatcagaagctttcatgtctgtctctggaa
agacataaagcaaaactttgcacgtttttttgcatgtttggattattctgtttcagttaacatattgttcttacgtttttatgtcagacagatttaaaccatgt
gactttcagccaccatatgactttagttttcttctaaaatcaagcaacccgttcactttatgcagctgatctgtttttgtcgccagtacacaaagagga
tgataaaaaatttaatatttggcacaaaagttcttctttttatattaaatgtctatttgtcttaacgatctgtgtacattttaattaaggtgcatctgggagta
gcttttagcagaggaacggcttatgattatatttcaaatccaggtgacgacatattcttacttcaaaaaaacagcaatgcaaataagagagtata
aattgtaatgtatattcaaccctcagtatactgcctattttgttataatgaaagtcctatattgagctttaattaaactctacacctatgggaattatttttctt
tataatgtcaagcatacactcgaatgactatgcgtgtatgtatataaaataaatataaatagatatatatttttttcctttacttttaccaccatcacttttg
ttgtttctggtttgtctttatgcaaaaacactgacacacacacgcacactaggctggatggtggatttccatttgcatctgctccaacaatatgaaaa
caaaactcaagttggcagtttgtagtattcagctctctctttgtctctctctcctgtgtaattctgtcatattttctttctcatgtgacgtgcatgatttcttaaa
gcaatagtcttcatcagcaaggagcggaggagagggatttggcataaactgtaaacctgaaaggctgtatgggaattgttgaatgcccgtag
ctgaagagagatttgctttgcctttaactgtccaccaggggtgctgacggcatccccgctattttgttttctttcgttttttaactcggagatgattgtttt
ctaaaagattgcttctctaacttgtcatcatggctttctaacacattttgactagataatgtacataatctgccaacttgattcattccat- 3’

cyfip1 3’ UTR

5’-

gcaccagtttgaagtggaagagatgggaaaagagagggaaatatttagcaacgtgtttaggaccagtttcactgtcacattctacttaatgatg
cctttcttatgccaccct
gtagtttctgcagagccagtaagttgccttgtgattggtcgagtgatttgatttgcaccaattactgcaccctactcaggctttggttaatcaggccaa
gatatgtttatgatgtacacaaacatggctcagttttactagcgtatttcaggttgatttttttttgtacacataaacacacacatacacacacactcgt
gccttattatagataaattgactataatcttttatatgttaatgatagcacagcactactcatgttttatacttgggaacagcagtggggtatggttcca
aaatggccaagtgggttttatcaaagggttatttaagcttttgctgtagtgcgagtccagcggtatttttttctatgtggtgttgaatgattgcatgcaagt
ttttttttcttctattatacttaataaaactttaagcgtagccaagttcttactcctcataaacgtgccttttt- 3’

cadm1b 3’ UTR

5’-

actggaactagacctgttagcttccagtgctgaacagcaaactgtggactgctgggtttgggaggaaggggttgtgggattcaatcaggctgga
ttcacacctgcgcag
ctgaagagacgctgctgccatcgagacggacggggtgtgggatggcagagcactaggagagctcaattttagaccgcttcaccatccaaca
cctcctgctggggccggttttgttccgtttaaacatttgctaagaattttgtgccttgttctgttcttactgaagttcccactttcatcaggacacccacaa
gctactgtctctccaatggtctgaatccacgttttttttttctctcctttcatttcatttttttaattgctagcacatcttaaagctctctctcatgctgttctgtctg
caggtctgaaagaaagccgcgcaccaagtttcgatgtaagattcagtcacagaatgatcgcttgggttgttttcacggattgattccaagtaatttt

atttggcaaattgcctgttgctctccttagtcccccagagaacgagttagagatgatagaaacctttttttctctctctttttttgtgaccaacaacattca gcagcagtattgcattgttgcaatatttattggatatactgtatgcgattatgatcagcttgtgttgatattagggctgtcaatcgaacacattactact attatttcgtttattaaatcattaaaatattacccaaatttggcaatgacatgacaaaatttatattattattattattatatacagctatggaaaaaatat taagactaattatgacatttcttactaaattaaaatgaaaaagttattatttagagcattgttttttttttttgcttgtttgtttttttctttaaaaaaaaaggtgct aaattttcagacatgttgctagccaaattcatttatatagaacatttcataaacagtaataattccaagtgctttacataaacaggaataaaagaa acaagtataagaaaataaaaaacaaattataacagtgaataaaagcagtttaaaatg- 3’

smFISH probe design

The *EGFP* smFISH probes were purchased from Stellaris LGC Biosearch Technologies. Probes consist of a set of pooled oligos with CAL Fluor® Red 610 Dye. *mbpa* smFISH probes were designed using the Stellaris RNA FISH Probe Designer tool by entering the zebrafish *mbpa* cDNA sequences obtained from Ensemble Genome Browser from transcript *mbpa-206* (GRCz11) (Table 3). Probes with highly repetitive sequences were removed. The probes were ordered with a CAL Fluor® Red 610 Dye. Probes were resuspended in Tris-EDTA, pH 8.0 and stored at a stock concentration of 12.5 µM at -20°C.

Table 3: Probe sequences for *mbpa*-206

Probe Name	Sequence 5'->3'	Probe Name	Sequence 5'->3'
Probe 1	CTTTGGATTGAGCGGAGAAG	Probe 13	AATCTTCAACCTGGGAGAAA
Probe 2	GTCCAGACTGTAGACCACTG	Probe 14	GATCTCGCTCTCCACCCAAA
Probe 3	CAGATCAACACCTAGAATGG	Probe 15	CTGGAGCACCATCTTCTGAG
Probe 4	CTCTGGACAAAACCCCTTCG	Probe 16	CTTCTCCAAGCAGGAAAACA
Probe 5	TGTCCTGGATCAAATCAGCA	Probe 17	GAGATGGAAGAGAGTGAAAT
Probe 6	TTCTTCGGAGGAGACAAGAA	Probe 18	CGGGAAGCAAAAACTTGAGA
Probe 7	AGAGACCCCACCACTCTT	Probe 19	ATGTCTGCCCTACAGACTCA
Probe 8	TCGTGCATTTCTTCAGGAGC	Probe 20	GTCGCAGCGAGTTTAACAGA
Probe 9	TCGTGCATTTCTTCAGGAGC	Probe 21	ACATTGGCCATCTTCGCTTC
Probe 10	TCGAGGTGGAGAGAACTATT	Probe 22	AGATAGAGATACAATCCAAG
Probe 11	CATTAGATCGCCACAGAGAC	Probe 23	TCTGTTGCTACATGCCTGCA
Probe 12	AAGGGAACAGAACACACTTT	Probe 24	TTACAGAAGCACGTGTTGAC

smFISH experimental procedure

The smFISH protocol was adapted from three published protocols: (Lyubimova *et al.*, 2013; Oka and Sato, 2015; Hauptmann, Lauter and Söll, 2016). First, larvae were sorted for EGFP expression and fixed O/N in 4% paraformaldehyde at 4°C. Larvae were embedded laterally in 1.5% agar, 5% sucrose

blocks and transferred to a 30% sucrose solution O/N at 4°C. Blocks were frozen on dry ice and sectioned with a Leica cryostat into 20 µm thick sections and placed on microscope slides. Slides were not allowed to dry more than 5 min before adding 4% paraformaldehyde to fix the tissue at RT for 10-20 min. The slides were quickly rinsed with 1X PBS twice. The tissue was permeabilized with 70% cold ethanol at -20^{0}C for 2 hours. Parafilm was placed over tissue to prevent evaporation at all incubation steps. The tissue was rehydrated with wash buffer (10% DI formamide, 2X SSC in molecular grade water) for 5 min at RT. From this point on, care was taken to protect the tissue and probes from light as much as possible. Hybridization Buffer was made: 2x SSC, 10% DI formamide, 25mg/mL tRNA, 50mg/mL bovine serum albumin, 200mM ribonucleoside vanadyl complex in DEPC water. Aliquots were made and stored at -20^{0}C. Probe was added to hybridization buffer 1:100 for a final concentration of 125 nM. As a control, slides were incubated in hybridization buffer with no probe. Slides were quickly rinsed with fresh wash buffer followed by 2 wash steps at 37^{0}C for 30 minutes. DAPI was added at 1:1000 concentration in wash buffer to the tissue for 7 min at RT. Slides were quickly rinsed twice with wash buffer. Finally, slides were mounted with Vectashield mounting media and a No. 1 coverslip and sealed with nail polish. All slides were stored and protected from light at 4^{0}C.

Whole mount in situ RNA hybridization

Control and TTX-injected larvae were hybridized with digoxygenin-labeled probe to detect *mbpa* mRNA and photographed using a compound microscope.

Microscopy

To image RNA localization in living animals, plasmids were injected with mRNA encoding Tol2 transposase into newly fertilized eggs. Injection solutions contained 5 µL 0.4 M KCl, 250 ng Tol2 mRNA and 125 ng pEXPR-*sox10:NLS-tdMCP-EGFP-sv40 3' UTR-tol2* plasmid and 125 ng pEXPR-*mbpa:mScarlet-CAAX-various 3' UTR-polyA-tol2*. Larvae were grown to 4 dpf and selected for good health and normal developmental patterns. Larvae were immobilized in 0.6% low-melt agarose with 0.06% tricaine. Images of single timepoint data were obtained using a Zeiss LSM 880 laser scanning confocal microscope equipped with a 40x, 1.3 NA oil immersion objective. Imaging was performed using Zeiss Zen Black software with the following parameters: 1024 x 1024 frame size, 1.03 µsec pixel dwell time, 16-bit depth, pinhole set to 1 Airy unit, 700 digital gain, 488 filter range 481-571, mScarlet filter range 605-695 and z intervals of 0.5 µm. All images of single cells were taken in the spinal cord of living zebrafish above the yolk extension. Cells were selected for imaging based on dual expression of EGFP and mScarlet-CAAX.

Images of smFISH experiments were obtained using a Zeiss LSM 880 with Airyscan confocal microscope and a Plan-Apochromat 63x objective, 1.4 NA oil immersion objective. The acquisition light path used Diode 405, Argon 488, HeNe 594 lasers, 405 beam splitter and 488/594 beam splitters, and Airyscan detector. Imaging was performed using Zeiss Zen Black software and parameters included: 1024 x 1024 frame size, 1.03usec pixel dwell time, 16-bit depth, 3x zoom, pinhole set to 1 Airy unit, line averaging was set to 2, 750 gain, and z intervals of 0.3 µm. All images of single cells were taken in the hindbrain of zebrafish larvae. Cells were selected for imaging based on expression of EGFP-CAAX and Quasar-610 fluorescence. Post-image processing was performed using Airyscan Processing set to 6.8.

Neuronal inhibition by tetrodotoxin (TTX)

We injected 2nL of tetrodotoxin (TTX) (0.5 mM) into the yolk of 2 dpf zebrafish embryos (Hines *et al.*, 2015). First, embryos were dechorionated and anesthetized in tricaine. Control embryos were uninjected and anesthetized in tricaine for equal lengths of time. TTX was delivered in a buffered solution containing 0.05% phenol red, 120 mM KCl, 30 mM HEPES, pH 7.3. Embryos were selected for experimental use if they had normal developmental morphologies and did not respond to touch or sound.

Semi-quantitative RT-PCR

RNA isolation was isolated from 4 dpf AB larvae and cDNA was synthesized as described above in the 3' UTR Cloning section.

Semi-quantitative RT-PCR was performed using TaqMan Universal PCR Master mix and custom designed primer/probe to target *mbpa, EGFP* or *rpl13a*, a housekeeping gene used for normalization. All procedures for creating PCR master mix were performed according to manufacturer's protocol. Each condition was completed using a minimum of three biological replicates and each biological replicate consisted of three technical replicates. To combine data from multiple replicates we used Step-One and Expression Suite software. Statistical analysis was performed in RStudio with Student's t-test.

QUANTIFICATION AND STATISTICAL ANALYSIS

Quantification of MS2 RNA localization

All images were processed and analyzed using ImageJ Fiji software. To analyze mRNA fluorescent intensity in sheath termini, we imaged single cells co-expressing NLS-MCP-EGFP and mScarlet-CAAX. Individual myelin sheaths were optically isolated by performing a maximum z projection of images collected at 0.5 µm intervals. Fluorescence intensity was measured by performing line scans across a

7 μm (± 0.3 μm) distance beginning at the terminal end of each sheath. Specifically, we drew each line in the mScarlet-CAAX channel to ensure we encompassed the edge of the myelin membrane. Gray values along each line (at 0.2 μm intervals) were measured in both channels. All measurements were combined into a Microsoft Excel file and imported into RStudio for further processing and analysis. In RStudio we used tidyverse and ggplot2 libraries to manipulate data and generate plots. To normalize fluorescence intensities in each sheath, we divided the raw gray value at each distance by the average gray values of all distances per sheath. To calculate the average mRNA fluorescence intensity among all myelin sheaths, we plotted the average normalized fluorescence intensity by distance. To calculate mRNA fluorescence intensities in myelin sheaths, we plotted the average fluorescent intensity of EGFP (raw gray values) for each sheath using the line scan measurements described above.

smFISH Quantification

All quantification was performed in ImageJ Fiji using a custom script created by Karlie Fedder (available upon request). First, z intervals were selected for individual cells or myelin tracts using the "Make Substack" feature in Fiji. Substacks for cell bodies included all z intervals for each soma. Substacks of myelin tracts in the hindbrain included 13 steps with an interval of 0.3 μm. Each substack was maximum z-projected. Background was subtracted using a 2.5 rolling ball. The image was then thresholded by taking 3 standard deviations above the mean fluorescence intensity with a size of 0.01-Infinity and circularity of 0.00-1.00. Using the maximum projection of the EGFP-CAAX channel, a region of interest (ROI) was drawn around each cell body using the freehand tool. Alternatively, for myelin ROIs, the rectangle tool was used to draw a square 100 x 100 pixels (4.39 μm x 4.39 μm). All thresholded signal was inspected manually for accuracy of thresholding parameters. Occasionally, threshold puncta fell on the border of the ROI and these were excluded from measurements. *mbpa* transcripts are highly expressed and counting individual puncta was not consistently reliable. Therefore, to measure mRNA abundance we calculated the density of signal in each ROI. Specifically, we overlaid the binary image on the maximum z projected image and calculated the density (area x average fluorescence intensity) using the "IntDen" measurement.

To obtain the average mRNA abundance per subcellular compartment, we calculated the average density for all signal in each ROI (cell bodies or myelin). All ROIs for each subcellular compartment were then averaged to calculate the average density per subcellular compartment.

Statistics

All statistics were performed in RStudio (version 1.1.456) using devtools and ggsignif packages. Specifically, tidyverse, ggsignif, readxl, RColorBrewer and ggpubr libraries were installed. All

statistically analyses were performed with ggpubr. Wilcoxon rank sum was performed for unpaired comparisons of two groups.

REFERENCES

Ainger, K. *et al.* (1993) 'Transport and localization of exogenous myelin basic protein mRNA microinjected into oligodendrocytes', *Journal of Cell Biology*, 123(2), pp. 431–441. doi: 10.1083/jcb.123.2.431.

Ainger, K. *et al.* (1997) 'Transport and localization elements in myelin basic protein mRNA', *Journal of Cell Biology*, 138(5), pp. 1077–1087. doi: 10.1083/jcb.138.5.1077.

Almeida, R. G. *et al.* (2011) 'Individual axons regulate the myelinating potential of single oligodendrocytes in vivo', *Development*. Oxford University Press for The Company of Biologists Limited, 138(20), pp. 4443–4450. doi: 10.1242/DEV.071001.

Banko, J. L. *et al.* (2005) 'The Translation Repressor 4E-BP2 Is Critical for eIF4F Complex Formation, Synaptic Plasticity, and Memory in the Hippocampus', *Journal of Neuroscience*. Society for Neuroscience, 25(42), pp. 9581–9590. doi: 10.1523/JNEUROSCI.2423-05.2005.

Bertrand, E. *et al.* (1998) 'Localization of ASH1 mRNA Particles in Living Yeast', *Molecular Cell*. Cell Press, 2(4), pp. 437–445. doi: 10.1016/S1097-2765(00)80143-4.

Briese, M. *et al.* (2016) 'Whole transcriptome profiling reveals the RNA content of motor axons', *Nucleic Acids Research*. Oxford University Press, 44(4), pp. e33–e33. doi: 10.1093/nar/gkv1027.

Buj, R. *et al.* (2013) 'A plasmid toolkit for cloning chimeric cDNAs encoding customized fusion proteins into any Gateway destination expression vector', *BMC Molecular Biology*. BioMed Central, 14(18), pp. 1–16. doi: 10.1186/1471-2199-14-18.

Buss, R. R., Bourque, C. W. and Drapeau, P. (2003) 'Membrane Properties Related to the Firing Behavior of Zebrafish Motoneurons', *Journal of Neurophysiology*. American Physiological SocietyBethesda, MD , 89(2), pp. 657–664. doi: 10.1152/jn.00324.2002.

Cajigas, I. J. *et al.* (2012) 'The Local Transcriptome in the Synaptic Neuropil Revealed by Deep Sequencing and High-Resolution Imaging', *Neuron*, 74(3), pp. 453–466. doi: 10.1016/j.neuron.

Campbell, P. D. *et al.* (2015) 'Dynamic visualization of transcription and RNA subcellular localization in zebrafish.', *Development (Cambridge, England)*, (March), pp. 1–7. doi: 10.1242/dev.118968.

Carson, J. H. *et al.* (1997) 'Translocation of myelin basic protein mRNA in oligodendrocytes requires microtubules and kinesin', *Cell Motility and the Cytoskeleton*, 38(4), pp. 318–328. doi: 10.1002/(SICI)1097-0169(1997)38:4<318::AID-CM2>3.0.CO;2-#.

Chong, S. Y. C. *et al.* (2012) 'Neurite outgrowth inhibitor Nogo-A establishes spatial segregation and extent of oligodendrocyte myelination.', *Proceedings of the National Academy of Sciences of the United States of America*. National Academy of Sciences, 109(4), pp. 1299–304. doi: 10.1073/pnas.1113540109.

Colman, D. R. (1982) 'Synthesis and incorporation of myelin polypeptides into CNS myelin', *The Journal of Cell Biology*, 95(2), pp. 598–608. doi: 10.1083/jcb.95.2.598.

Czopka, T., Ffrench-Constant, C. and Lyons, D. (2013) 'Individual Oligodendrocytes Have Only a Few Hours in which to Generate New Myelin Sheaths In Vivo', *Developmental Cell*, 25(6), pp. 599–609. doi: 10.1016/j.devcel.2013.05.013.

Etxeberria, A. *et al.* (2016) 'Dynamic Modulation of Myelination in Response to Visual Stimuli Alters Optic Nerve Conduction Velocity.', *The Journal of neuroscience : the official journal of the Society for Neuroscience*. Society for Neuroscience, 36(26), pp. 6937–48. doi: 10.1523/JNEUROSCI.0908-16.2016.

Farris, S. *et al.* (2014) 'Selective Localization of Arc mRNA in Dendrites Involves Activity-and Translation-Dependent mRNA Degradation', *The Journal of Neuroscience*, 34(13), pp. 4481–4493. doi: 10.1523/JNEUROSCI.4944-13.2014.

Femino, A. M. *et al.* (1998) 'Visualization of single RNA transcripts in situ', *Science*, 280, pp. 585–590. doi: 10.1126/science.280.5363.585.

Fitzgerald, M. and Shenk, T. (1980) 'THE SITE AT WHICH LATE mRNAs ARE POLYADENYLATED IS ALTERED IN SV40 MUTANT dl882', *Annals of the New York Academy of Sciences*. John Wiley & Sons, Ltd (10.1111), 354(1 Genetic Varia), pp. 53–59. doi: 10.1111/j.1749-6632.1980.tb27957.x.

Fusco, D. *et al.* (2003) 'Single mRNA Molecules Demonstrate Probabilistic Movement in Living Mammalian Cells', *Current Biology*, 13(2), pp. 161–167. doi: 10.1016/S0960-9822(02)01436-7.

Gibson, E. M. *et al.* (2014) 'Neuronal activity promotes oligodendrogenesis and adaptive myelination in the mammalian brain.', *Science (New York, N.Y.)*, 344(6183). doi: 10.1126/science.1252304.

Gkogkas, C. G. *et al.* (2012) 'Autism-related deficits via dysregulated eIF4E-dependent translational control', *Nature*. Nature Publishing Group, 493(7432), pp. 371–377. doi: 10.1038/nature11628.

Hafner, A.-S. *et al.* (2019) 'Local protein synthesis is a ubiquitous feature of neuronal pre- and postsynaptic compartments', *Science (New York, N.Y.)*. American Association for the Advancement of Science, 364(650), pp. 1–12. doi: 10.1126/science.aau3644.

Halstead, J. M. *et al.* (2015) 'An RNA biosensor for imaging the first round of translation from single cells to living animals', *Science (New York, N.Y.)*. NIH Public Access, 347(6228), pp. 1367–671. doi: 10.1126/science.aaa3380.

Herbert, A. L. *et al.* (2017) 'Dynein/dynactin is necessary for anterograde transport of Mbp mRNA in oligodendrocytes and for myelination in vivo.', *Proceedings of the National Academy of Sciences of the United States of America*. National Academy of Sciences, 114(43), pp. E9153–E9162. doi: 10.1073/pnas.1711088114.

Hines, J. H. *et al.* (2015) 'Neuronal activity biases axon selection for myelination in vivo', *Nature Neuroscience*, 18(5), pp. 683–689. doi: 10.1038/nn.3992.

Huber, K. M., Kayser, M. S. and Bear, M. F. (2000) 'Role for rapid dendritic protein synthesis in hippocampal mGluR-dependent long-term depression.', *Science (New York, N.Y.)*. American Association for the Advancement of Science, 288(5469), pp. 1254–7. doi: 10.1126/SCIENCE.288.5469.1254.

Kang, H. and Schuman, E. M. (1996) 'A Requirement for Local Protein Synthesis in Neurotrophin-Induced Hippocampal Synaptic Plasticity', *Science*, 273(5280), pp. 1402–1406.

Koudelka, S. *et al.* (2016) 'Individual Neuronal Subtypes Exhibit Diversity in CNS Myelination Mediated by Synaptic Vesicle Release', *Current Biology*. Cell Press, 26(11), pp. 1447–1455. doi: 10.1016/J.CUB.2016.03.070.

Krauss, J. *et al.* (2009) 'Myosin-V Regulates oskar mRNA Localization in the Drosophila Oocyte', *Current Biology*. Cell Press, 19(12), pp. 1058–1063. doi: 10.1016/J.CUB.2009.04.062.

Kristensson, K. *et al.* (1986) 'The Journal of Histochemistry Expression of Myelin Basic Protein Gene in the Developing Rat Brain as Revealed by in Situ Hybridization', *The Journal of Histochemistry and Cytochemistry*, 34(4), pp. 467–473. Available at: https://journals.sagepub.com/doi/pdf/10.1177/34.4.2419396 (Accessed: 2 April 2019).

Kwan, K. M. *et al.* (2007) 'The Tol2kit: a multisite gateway-based construction kit for Tol2 transposon transgenesis constructs', *Dev Dyn*, 236(11), pp. 3088–3099.

Leung, K.-M. *et al.* (2006) 'Asymmetrical β-actin mRNA translation in growth cones mediates attractive turning to netrin-1', *Nature Neuroscience*. Nature Publishing Group, 9(10), pp. 1247–1256. doi: 10.1038/nn1775.

Li, Z. *et al.* (2001) 'The fragile X mental retardation protein inhibits translation via interacting with mRNA', *Nucleic Acids Research*. Narnia, 29(11), pp. 2276–2283. doi: 10.1093/nar/29.11.2276.

Lunn, K. F., Baas, P. W. and Duncan, I. D. (1997) 'Microtubule Organization and Stability in the Oligodendrocyte', *Journal of Neuroscience*, 17(13), pp. 4921–4932. Available at: http://www.jneurosci.org/content/jneuro/17/13/4921.full.pdf (Accessed: 27 April 2017).

Lyons, D. a *et al.* (2009) 'Kif1b is essential for mRNA localization in oligodendrocytes and development of myelinated axons.', *Nature genetics*, 41(7), pp. 854–8. doi: 10.1038/ng.376.

Mensch, S. *et al.* (2015) 'Synaptic vesicle release regulates the number of myelin sheaths made by individual oligodendrocytes in vivo', *Natural neuroscience*, 18(5), pp. 628–630. doi: 10.1038/nn.3991.Synaptic.

Minis, A. *et al.* (2014) 'Subcellular transcriptomics-Dissection of the mRNA composition in the axonal compartment of sensory neurons', *Developmental Neurobiology*. John Wiley & Sons, Ltd, 74(3), pp. 365–381. doi: 10.1002/dneu.22140.

Mitew, S. *et al.* (2018) 'Pharmacogenetic stimulation of neuronal activity increases myelination in an axon-specific manner', *Nature Communications*. Nature Publishing Group, 9(1), p. 306. doi: 10.1038/s41467-017-02719-2.

Morisaki, T. *et al.* (2016) 'Real-time quantification of single RNA translation dynamics in living cells.', *Science (New York, N.Y.)*. American Association for the Advancement of Science, 352(6292), pp. 1425–9. doi: 10.1126/science.aaf0899.

Murtie, J. C., Macklin, W. B. and Corfas, G. (2007) 'Morphometric analysis of oligodendrocytes in the adult mouse frontal cortex', *Journal of Neuroscience Research*. John Wiley & Sons, Ltd, 85, pp. 2080–2086. doi: 10.1002/jnr.21339.

Nawaz, S. *et al.* (2015) 'Actin Filament Turnover Drives Leading Edge Growth during Myelin Sheath Formation in the Central Nervous System', *Developmental Cell*. Europe PMC Funders, 34(2), pp. 139–151. doi: 10.1016/j.devcel.2015.05.013.

Pacey, L. K. K. *et al.* (2013) 'Delayed myelination in a mouse model of fragile X syndrome', *Human Molecular Genetics*. Narnia, 22(19), pp. 3920–3930. doi: 10.1093/hmg/ddt246.

Pause, A. *et al.* (1994) 'Insulin-dependent stimulation of protein synthesis by phosphorylation of a regulator of 5'-cap function', *Nature*. Nature Publishing Group, 371(6500), pp. 762–767. doi: 10.1038/371762a0.

Pichon, X. *et al.* (2016) 'Visualization of single endogenous polysomes reveals the dynamics of translation in live human cells.', *The Journal of cell biology*. Rockefeller University Press, 214(6), pp. 769–81. doi: 10.1083/jcb.201605024.

Raj, A. *et al.* (2008) 'Imaging individual mRNA molecules using multiple singly labeled probes', *Nature Methods*, 5(10), pp. 877–879. doi: 10.1038/nmeth.1253.

Snaidero, N. *et al.* (2014) 'Myelin Membrane Wrapping of CNS Axons by PI(3,4,5)P3-Dependent Polarized Growth at the Inner Tongue', *Cell*, 156(1–2), pp. 277–290. doi: 10.1016/j.cell.2013.11.044.

Steward, O. and Worley, P. F. (2001) 'Selective Targeting of Newly Synthesized Arc mRNA to Active Synapses Requires NMDA Receptor Activation', *Neuron*. Cell Press, 30(1), pp. 227–240. doi: 10.1016/S0896-6273(01)00275-6.

Taliaferro, J. M. *et al.* (2016) 'Distal Alternative Last Exons Localize mRNAs to Neural Projections', *Molecular Cell*, 61, pp. 821–833. doi: 10.1016/j.molcel.2016.01.020.

Taylor, A. M. *et al.* (2009) 'Axonal mRNA in uninjured and regenerating cortical mammalian axons.', *The Journal of neuroscience : the official journal of the Society for Neuroscience*. Society for Neuroscience, 29(15), pp. 4697–707. doi: 10.1523/JNEUROSCI.6130-08.2009.

Thakurela, S., Garding, A., Jung, Ramona B, *et al.* (2016) 'The transcriptome of mouse central nervous system myelin-supplement', *Scientific reports*, 6, p. 25828. doi: 10.1038/srep25828.

Thakurela, S., Garding, A., Jung, Ramona B., *et al.* (2016) 'The transcriptome of mouse central nervous system myelin', *Scientific Reports*. Nature Publishing Group, 6(1), p. 25828. doi: 10.1038/srep25828.

Tiruchinapalli, D. M. *et al.* (2003) 'Activity-dependent trafficking and dynamic localization of zipcode binding protein 1 and beta-actin mRNA in dendrites and spines of hippocampal neurons', *The Journal of neuroscience : the official journal of the Society for Neuroscience*. Society for Neuroscience, 23(8), pp. 3251–61. doi: 10.1523/JNEUROSCI.23-08-03251.2003.

Tongiorgi, E., Righi, M. and Cattaneo, A. (1997) 'Activity-Dependent Dendritic Targeting of BDNF and TrkB mRNAs in Hippocampal Neurons', *Journal of Neuroscience*. Society for Neuroscience, 17(24), pp. 9492–9505. doi: 10.1523/JNEUROSCI.17-24-09492.1997.

Torvund-Jensen, J. *et al.* (2018) 'The 3'UTRs of Myelin Basic Protein mRNAs Regulate Transport, Local Translation and Sensitivity to Neuronal Activity in Zebrafish', *Frontiers in Molecular Neuroscience*. Frontiers, 11, p. 185. doi: 10.3389/fnmol.2018.00185.

Trapp, B. D. *et al.* (1987) 'Spatial segregation of mRNA encoding myelin-specific proteins (oligodendrocytes/Schwann cells/in situ hybridization/immunocytochemistry)', *Neurobiology*, 84, pp. 7773–7777. Available at: https://www.pnas.org/content/pnas/84/21/7773.full.pdf (Accessed: 26 December 2018).

Wake, H., Lee, P. R. and Fields, R. D. (2011) 'Control of Local Protein Synthesis and Initial Events in Myelination by Action Potentials', *Science*, 333(6049), pp. 1647–1651. doi: 10.1126/science.1206998.

Wang, C. *et al.* (2016) 'Real-Time Imaging of Translation on Single mRNA Transcripts in Live Cells', *Cell*, 165(4), pp. 990–1001. doi: 10.1016/j.cell.2016.04.040.

Wang, H. *et al.* (2003) 'Developmentally-programmed FMRP expression in oligodendrocytes: a potential role of FMRP in regulating translation in oligodendroglia progenitors', *Human Molecular Genetics*. Narnia, 13(1), pp. 79–89. doi: 10.1093/hmg/ddh009.

Yan, X. *et al.* (2016) 'Dynamics of Translation of Single mRNA Molecules In Vivo.', *Cell*. Elsevier, 165(4), pp. 976–89. doi: 10.1016/j.cell.2016.04.034.

Yoon, Y. J. *et al.* (2016) 'Glutamate-induced RNA localization and translation in neurons', *Proceedings of the National Academy of Sciences*, 113(44), pp. E6877–E6886. doi: 10.1073/pnas.1614267113.

Yoshimura, A. *et al.* (2006) 'Myosin-Va facilitates the accumulation of mRNA/protein complex in dendritic spines', *Current biology : CB*. Elsevier, 16(23), pp. 2345–2351. doi: 10.1016/j.cub.2006.10.024.

Zalfa, F. *et al.* (2003) 'The Fragile X Syndrome Protein FMRP Associates with BC1 RNA and Regulates the Translation of Specific mRNAs at Synapses', *Cell*. Cell Press, 112(3), pp. 317–327. doi: 10.1016/S0092-8674(03)00079-5.

Zalfa, F. *et al.* (2007) 'A new function for the fragile X mental retardation protein in regulation of PSD-95 mRNA stability', *Nature Neuroscience*. Nature Publishing Group, 10(5), pp. 578–587. doi: 10.1038/nn1893.

Zhang, X. hui and Poo, M. (2002) 'Localized synaptic potentiation by BDNF requires local protein synthesis in the developing axon.', *Neuron*. Elsevier, 36(4), pp. 675–88. doi: 10.1016/S0896-6273(02)01023-1.

Zhang, Y. *et al.* (2014) 'An RNA-sequencing transcriptome and splicing database of glia, neurons, and vascular cells of the cerebral cortex', *Journal of Neuroscience*, 34(36), pp. 11929–11947. doi: 10.1523/JNEUROSCI.1860-14.2014.

Zivraj, K. H. *et al.* (2010) 'Cellular/Molecular Subcellular Profiling Reveals Distinct and Developmentally Regulated Repertoire of Growth Cone mRNAs'. doi: 10.1523/JNEUROSCI.1800-10.2010.

Zuchero, J. B. *et al.* (2015) 'CNS Myelin Wrapping Is Driven by Actin Disassembly', *DEVCEL*, 34, pp. 152–167. doi: 10.1016/j.devcel.2015.06.011.